Increasing the Ionization Energy Offset to Increase the Quantum Efficiency in Non-Fullerene Acceptor-Based Organic Solar Cells: How Far Can We

ADVANCED MATERIALS INTERFACES
Open Access
www.advmatinterfaces.de

Increasing the Ionization Energy Offset to Increase the Quantum Efficiency in Non-Fullerene Acceptor-Based Organic Solar Cells: How Far Can We Go?

Julien Gorenflot, Wejdan Alsufyani, Maryam Alqurashi, Sri Harish Kumar Paleti, Derya Baran, and Frédéric Laquai*

Molecular engineering of organic semiconductors provides a virtually unlimited number of possible structures, yet only a handful of combinations lead to state-of-the-art efficiencies in photovoltaic applications. Thus, design rules that guide material development are needed. One such design principle is that in a bulk heterojunction consisting of an electron donor and lower bandgap acceptor an offset (ΔIE) of at least 0.45 eV is required between both materials ionization energies to overcome energy level bending at the donor–acceptor interface, in turn maximizing the charge separation yield and the cell's internal quantum efficiency. The present work studies energy losses associated with ΔIE and, based on 24 blends, finds that losses are minimal up to a ΔIE of 0.6 eV. Electroluminescence spectroscopy shows that low energy losses are achieved when the charge transfer state energy (E_{CT}) is similar to the acceptor's optical bandgap (E_g^A). Further ΔIE increase lowers E_{CT} with respect to E_g^A, thus decreasing V_{OC}. Within that 0.45–0.6 eV ΔIE sweet range, the fill factor FF, hence the power conversion efficiency, increases only marginally as the FF is often already close to maximal for ΔIE = 0.45 eV. The results are extended to 76 binary and ternary blends.

1. Introduction

Organic photovoltaics (OPV) relies on careful selection of specific organic semiconductor materials with highly-engineered properties from the pool of sheer unlimited materials. However, only a few result in high device efficiencies, and it took more than 30 years of empirical optimization[1,2] from the first proof of concept by Tang delivering only 1% power conversion efficiency (PCE) in 1986,[3] to develop the latest Y-series of non-fullerene acceptor (NFA) molecules[4,5] that now yield efficiencies close to 20%.[6–11]

The field of OPV has always been in need of design principles that could guide the synthesis of new molecules. In parallel to molecular engineering, our understanding of the photophysics governing the solar cell performances has considerably increased in the last 30 years, and such sets of meaningful design rules have started to solidify.[12–15] Furthermore, first principle-based computational materials chemistry has progressed to the point where energy levels can not only be computed in the gas phase, but also extrapolated to films, which allows for screening many potential structures of OPV materials and selecting the most promising for synthesis.[14]

For low-bandgap NFA-based solar cells, we previously showed that the acceptor's ionization energy has to be ≈0.45 eV higher (more negative with respect to vacuum) than that of the donor, to maximize exciton quenching by hole transfer from the acceptor to the donor and in turn the solar cells' internal quantum efficiency (IQE).[12,14] We showed that this hole transfer efficiency sets a ceiling to the solar cells' IQE. The 0.45 eV ionization energy offset ΔIE was shown to be required to counterbalance energy level bending (measured as bias potential B) at the donor-acceptor (D/A) interface, which increases the energy of the interfacial charge transfer (CT) and thus impedes the exciton-to-CT-state transition if ΔIE is low.[12,14,16] The interfacial energy level bending is a consequence of the energetic landscape in NFA-based blends, more specifically the interaction of charges with the surrounding molecules' (NFA and donors) intrinsic quadrupole moments.[12,14,15,17,18] On the other hand, the bending facilitates charge separation (CT to free charge conversion) and diffusion from the interface, explaining the observation of barrier-less charge generation in the top-performing OPV systems.[19]

Very recently, we reported that the same applies to ternary blends, composed of one donor and two acceptors.[20] Interestingly, the IQE follows the average IE of both acceptors weighted by their blending (weight) ratio.[20] While

J. Gorenflot, W. Alsufyani, M. Alqurashi, S. H. K. Paleti,[+] D. Baran, F. Laquai
KAUST Solar Center
Physical Science and Engineering Division
Applied Physics Program
King Abdullah University of Science and Technology
Thuwal 23955–6900, Kingdom of Saudi Arabia
E-mail: julien.gorenflot@kaust.edu.sa

The ORCID identification number(s) for the author(s) of this article can be found under https://doi.org/10.1002/admi.202202515.

[+]Present address: Department of Chemistry and Chemical Engineering, Chalmers University of Technology, Göteborg 41296, Sweden

DOI: 10.1002/admi.202202515

ADVANCED MATERIALS INTERFACES
Open Access
www.advmatinterfaces.de

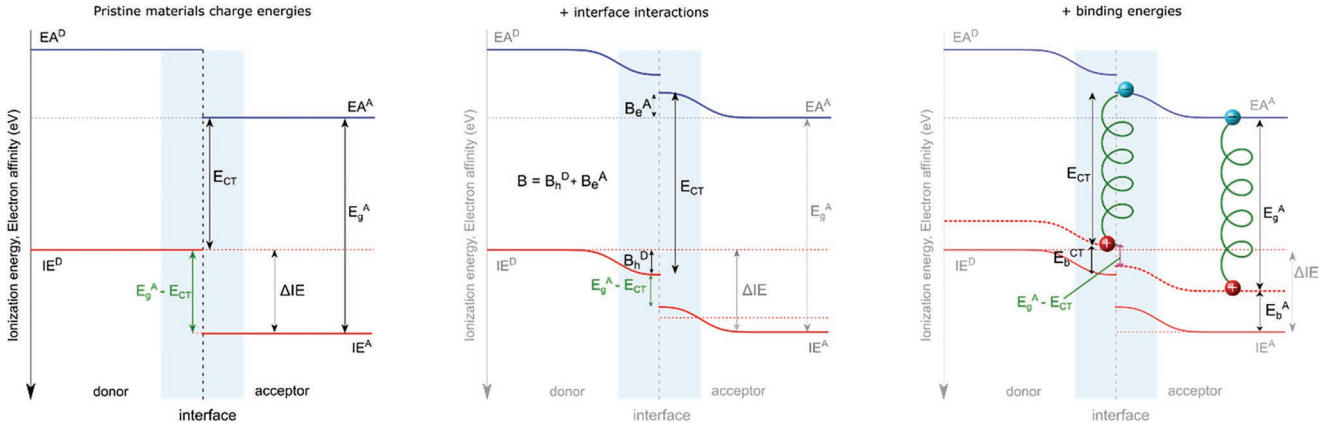

Figure 1. Schematic representation of the difference between the acceptor's exciton energy E_g^A and the interfacial CT state energy. E_{CT}, and their relation to the ionization energy offset ΔIE. B is the interface energy level bending, E_b the exciton or CT-state binding energy. The superscripts D and A stand for electron donor and electron acceptor, respectively, and the subscripts h and e for hole and electron, respectively.

here ionization energies were determined by photoemission spectroscopy,[21] a similar trend was found using cyclic voltammetry, however, with a lower ΔIE threshold.[22] This is likely due to the fact that cyclic voltammetry measurement tends to find much deeper IE for the donors, hence much lower offsets (for example for PBDB-T:Y6, in which ΔIE is close to 0 from CV measurements, but ≈0.5 eV from photoelectron spectroscopy measurements).[23] We have recently discussed this issue in details,[21] here we will use solely IE and electron affinity (EA) levels determined from photoemission spectroscopy.

We note also that Li et al. recently explained the peculiar interfacial energetic landscape by accounting for vacuum level shifts due to the presence of interfacial dipoles observed in bilayer films.[24] Vacuum level shifts modifies the energy of interface excited species (CT-states) relatively to neat material excitons similarly to energy level bending. As such it has identical effect on charge transfer and energy losses, however, it may not explain the barrier-less charge separation, unless this shift is limited to the D/A interface region. In the current work we focus on the energy levels bending explanation, while keeping in mind that vacuum level shift would probably be able to explain the experimental results as well. Most likely both effects play a role.

While this design rule: ΔIE > 0.45 eV enables to maximize the IQE, and through it the short circuit current j_{SC}, we wanted here to evaluate its impact on the cells power conversion efficiency, by studying whether ΔIE could be increased without negatively impacting the open circuit voltage (V_{OC}), and if yes, how far. Indeed, by increasing IE^A to increase ΔIE, we also increase the NFA's electron affinity EA^A, thus reducing the energy of the interfacial CT state. At the electron donor/electron acceptor (D/A) interface, recombination of charges occurs and consequently the interfacial CT state energy determines the open circuit voltage V_{OC}. Note that here we focus on systems in which the acceptor is the lower bandgap material, as is the case for most high performance OPV blends. However, we would expect similar observations in systems where the donor has the lowest bandgap, just replacing ionization energies by electron affinities and the acceptor's optical bandgap by that of the donor.[21]

We determined the minimum total energy loss according to $\Delta V_{OC} = E_g^A - eV_{OC}$, with E_g^A the acceptor's optical bandgap energy and V_{OC} the solar cell's open circuit voltage under 1 sun illumination. We found that as long as the interfacial CT state energy E_{CT} is lower than E_g^A, ΔV_{OC} is governed by E_{CT} reduced by the recombination-induced energy losses (radiative and non-radiative losses). However, here we particularly focus on the interfacial CT state energetics and its impact on Voc.

As shown in **Figure 1**, energy losses are related to ΔIE: i) considering the energy levels of separated charges in both materials as independent gives: $E_{CT} - E_g^A = EA^A - IE^D - E_g^A = \Delta IE$. ii) Including energy level bending at the donor–acceptor interface measured by B changes this difference to: $E_{CT} - E_g^A = \Delta IE - B$. iii) Finally, taking into account the acceptor exciton binding energy E_b^A and the CT state binding energy E_b^{CT}, we obtain: $E_{CT} - E_g^A = \Delta IE - B - E_b^A + E_b^{CT} = \Delta IE - B - \Delta E_b$.[25,26]

Here, we evaluated the energetic losses in the systems previously reported by us[12] and added several more blends, in total 24 D:A systems. The molecular structures are shown in Scheme S1, Supporting Information, their full names, suppliers, and energy levels are listed in Table S1, Supporting Information. We calculated ΔV_{OC} for all systems and rationalized the energetic losses with respect to ΔIE of each system. Electroluminescence spectroscopy on a large subset of systems was used to determine their interfacial CT state energy. To test the generality of our findings, we finally extend the analysis to more systems from literature including ternary blends for a total of 74 blends.

2. Results and Discussion

2.1. Evolution of Quantum Efficiency and Energy Losses with the IE Offset

As shown in **Figure 2** both the internal quantum efficiency (IQE) and the energy losses ΔV_{OC} in the solar cells increase with ΔIE. However, the IQE (measured in short circuit conditions) is maximized and plateaus for ΔIE > 0.45 eV,[12] while the energy losses remain constant up to 0.6 eV. This indicates that a "sweet spot" of ΔIE values exists between 0.45 and 0.6 eV, which

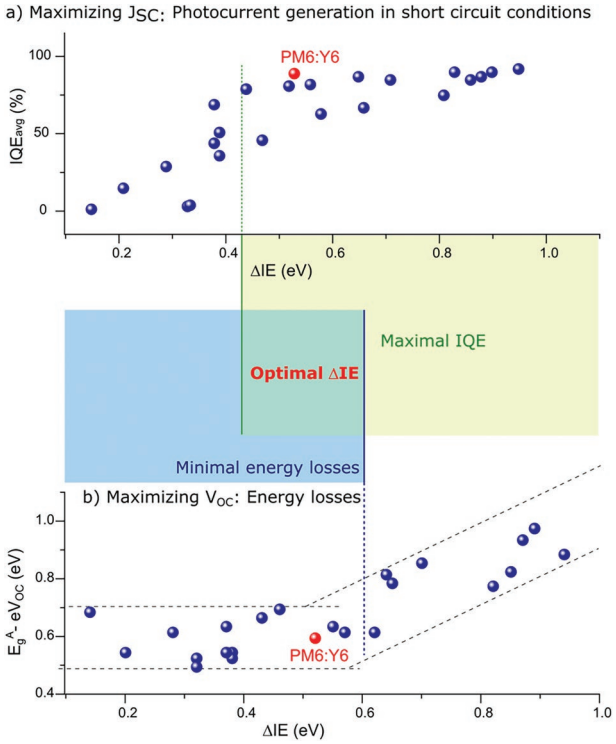

Figure 2. a) IQE and b) energy losses versus ΔIE. Data from Karuthedath et al.[12,27] The dashed line in panel b) stress the two observed regimes: stable energy losses below ≈0.6 eV and their raise equal to the raise of ΔIE (slope 1) for ΔIE > 0.6 eV.

enable a high charge generation yields, while keeping energy losses at a minimum. Unsurprisingly, the ΔIE of state-of-the-art organic solar cells including PM6:Y6 falls into this region. Further details of the blends represented by each data point and the corresponding solar cell figures of merit can be found in the supporting information, Figure S1 and Table S2, Supporting Information. Importantly, for ΔIE > 0.6 eV, the energy losses increase with ΔIE (see guides to the eye with unity slope in Figure 2b). This corresponds to the anticipated evolution of E_{CT} as schematized in Figure 1, with the difference that experimentally the ΔV_{OC} increase starts only for ΔIE > 0.6 eV.

2.2. Charge Transfer State Energy and the Limit of Low Energy Losses

In order to further understand the energy losses, we determined the charge transfer state energy from the blends' electroluminescence (EL) spectra from which the EL from neat acceptor devices was subtracted. The part of the EL spectra not originating from the acceptor itself was fitted by a Gaussian according to the method reported by Vandewal et al.,[28] giving as a full fitting equation for the reduced electroluminescence spectra rEL(E):

$$rEL(E) = \frac{EL(E)}{E} = \frac{f_1}{\sqrt{4\pi k_B T \lambda_{RO}}} e^{\frac{-(E_{CT}-\lambda_{RO}-E)^2}{4\lambda_{RO}k_B T}} + f_2 rEL_{acceptor}(E) \quad (1)$$

Where E is the photon energy, EL(E) is the measured EL spectrum converted to energy axis (see experimental section), λ_{RO} the reorganization energy associated with the CT to ground state electronic transition, k_BT the ambient thermal energy, $rEL_{acceptor}(E)$ the reduced electroluminescence spectra obtained from devices having the neat acceptor as active layer, and f_1 and f_2 fitting coefficient controlling the relative amplitude of the pristine and CT emissions in the blend. The EL spectra and corresponding fits can be found in Figures S2–S4, Supporting Information.

Historically, E_{CT} of fullerene acceptor-based blends has been determined using both the emission and the absorption of interface states.[28] The latter being probed using sensitive external quantum efficiency spectroscopy. This approach was still used here for DR3:$PC_{71}BM$ (Figure S2, Supporting Information and[12]). It can however not be applied to NFA-based blends as NFA absorb much more strongly, and, at energies much closer to E_{CT}. This results in the CT absorption being generally orders of magnitude lower than the low energy tail of the acceptor's absorption, and as such, impossible to identify in the EQE spectra.[29]

Focusing now on the emission only, Eisner et al.[30] have proposed to use up to three Gaussian to fit the neat acceptor and CT emissions, respectively. This approach presents the drawback of using nine free parameters, including E_{CT}, thus requiring additional data (injection current dependence of the spectra in the case of[30]) to ensure the unicity of the set of parameters. An alternative similar to ours was recently used by Perdigón-Toro et al.,[29] in which the pristine acceptor component of the EL was obtained by probing the photoluminescence (PL) on the blend device, the CT component of the emission being thus obtained by subtracting this PL from the EL.

Finally, it has long been considered that E_{CT} could be obtained by extrapolating V_{OC} to a temperature of 0 K.[28,31] However, there is a growing list of evidences that E_{CT} itself is temperature dependent, due to the influence of disorder,[32–35] and that E_{CT} (0 K) = V_{OC} (0 K) would be different from E_{CT} at room temperature.

Figure 3 shows the difference between the optical bandgap (photon energy) E_g^A and the charge transfer (interface) state energy E_{CT}. We note that here as well two regimes can be distinguished that determine the total energy loss ΔV_{OC}: i) up to ΔIE ≈ 0.6 eV, E_{CT} is found to be equal to E_g^A ($E_g^A - E_{CT}$, within a range of −50 to 70 meV with only two outliers ≈110 meV) and independent of ΔIE. ii) For ΔIE > 0.6 eV, E_{CT} increases with ΔIE and with a slope of 1, in other words, the increase of E_{CT} follows ΔIE. This clearly indicates that the observed evolution of V_{OC} with ΔIE in that range is due to the evolution of E_{CT}. In the following, we examine those two regimes more closely. Further details of the investigated systems can be found in Figure S6, Supporting Information.

Looking at the interfacial energetic landscape as shown in Figure 1, we expect the CT (interfacial) state energy to be larger than the acceptor's bandgap for low ΔIE systems. However, the experimental results (Figure 3) indicate that upon decreasing ΔIE, E_{CT} does increase until it reaches E_g^A, yet it does not become lower, in other words, $E_{CT} - E_g^A$ decreases to 0, but does not become negative. Two reasons may account for this observation: first, we probe E_{CT} using

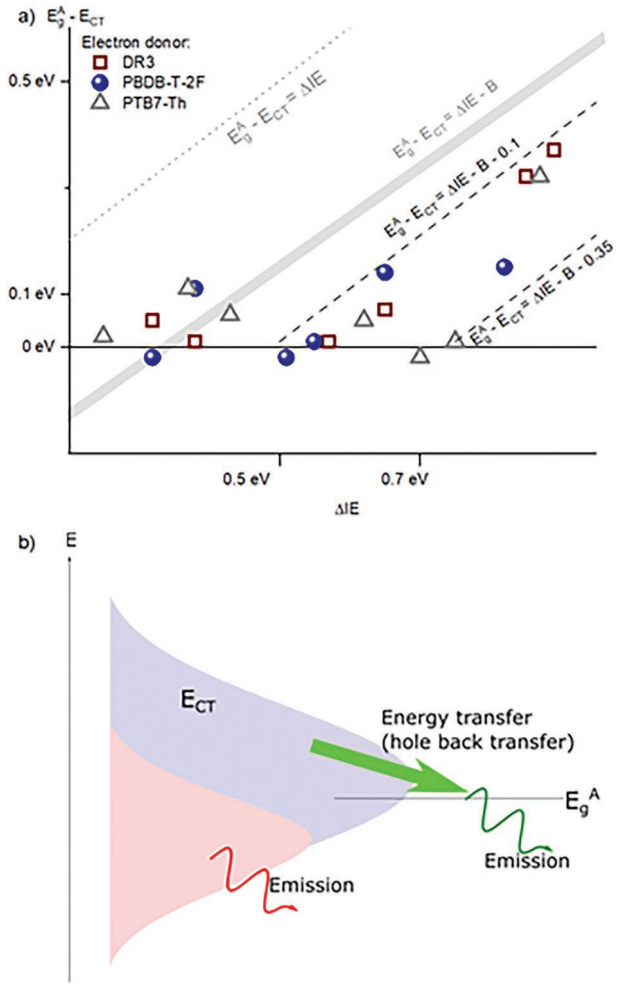

Figure 3. a) Energy losses from singlet (E_g^A) to interface state (E_{CT}): E_{CT} was obtained by fitting electroluminescence spectra (see Figures S2–S4, Supporting Information). The different lines correspond to the models presented in Figure 1: i) dotted line: no interface bending, no binding energy. ii) grayed areas: interface bending only (for average bending B between 0.37 and 0.39 eV as reported by Karuthedath et al.[12] for those systems). iii) dashed lines: interface bending and binding energy difference, for $B = 0.39$ eV and a difference ΔE_b between the acceptor exciton. and the interface state binding energies of 100 and 350 meV, respectively. The acceptor for each point can be found in Figure S6, Supporting Information. Data taken from[12,27] and[36] plus a few new measurements and corrections (details in Table S3, Supporting Information). b) Schematic representation of the excitation transfer between the charge transfer density of state and the acceptor singlet exciton level (represented as a discrete non-disordered level for sake of simplicity).

EL, however, as illustrated in Figure 3b, when the interfacial (CT) state energy becomes larger than the acceptor's exciton energy, the CT state can transfer to the acceptor, and thus the EL primarily stems from the acceptor. As mentioned, in our analysis the acceptor's emission is subtracted. Consequently, what is left from the emission is the fraction coming from the E_{CT} distribution, whose energy is lower than E_g^A. This is consistent with our observation that the Gaussian width of the CT emission is rather low for the lowest IE offset systems (E_{CT} < 0.5 eV, see Figure S3b, Supporting Information). This Gaussian width is represented by the fit parameter λ_{RO}, which in principle represents the reorganization energy corresponding to the CT state to ground state transition, while in reality it also includes the energetic disorder, if not specifically accounted for.[32–35] In that case, the average E_{CT} would be higher than E_g^A, but the higher energy CT-states transfer to the acceptor and thus are not visible in EL spectroscopy. Second, the interface state and the acceptor exciton being isoenergetic, hybridize:[30,37–40] the interface (CT) state thus becomes a CT-LE^A hybrid state, with the local acceptor component LE^A potentially becoming predominant as the CT state energy (without hybridization) increases and thus, the hybrid state emission becomes virtually similar to that of the acceptor's local excitonic state. In both cases, recombination occurs through the acceptor exited state, resp. the hybrid state having a large LE^A component, as a consequence the position of the pure CT state/component becomes unimportant for V_{OC}.

Looking at the systems with ΔIE > 0.6 eV, the decrease of E_{CT} (relative to the acceptors optical bandgap) follows exactly the increase of ΔIE, as expected from the three models presented in Figure 1. However, the ΔIE at which E_{CT} reaches E_g^A cannot be explained by only considering the average interface energy level bending B extracted from the ΔIE-dependence of the IQE.[12] Instead, this transition is shifted to higher energy by a value comprised between as little as 100 and as much as 350 meV, which we attribute to a lower binding energy of the CT states compared to the acceptor's singlet state energy. Most of the ΔE_b are between 100 to 150 meV, which is similar to the difference of 120 meV between the binding energy of a MDMO-PPV* exciton and that of a MDMO-PPV$^+$:PC$_{60}$BM$^-$ charge transfer state as experimentally found by Kern et al.[26]

We note that our EL spectra were not corrected for the spectrally-dependent coupling of the emitted light out of the devices,[41] and as such, our E_{CT} are rough estimates. However, the agreement of the evolution of $E_g - E_{CT}$ with ΔIE, with the evolution observed for $E_g - V_{OC}$ indicate that those estimate already give a good impression of the role of interface states on the energy losses.

2.3. Evolution of Quantum Efficiencies in the Low Energy Loss Range: Fill Factor and Field Dependent Generation

The fact that a quantitative hole transfer and IQE close to unity can be obtained in the range of ΔIE 0.45–0.6 eV is unexpected,[12] considering that the interface CT state energy is larger than the acceptor's exciton energy. This is in particular in contrast with the results by Nakano et al.[31] who found that, while the interface state energy was indeed the determining energy level for photocurrent generation, an offset of 0.2–0.3 eV was required between E_{CT} and E_g for efficient charge transfer. We attribute this difference to either the different E_{CT} determination methods they used, or to the fact that their study was carried out on bilayers. On the other hand, the result is in agreement with the work of Zhong et al. that found efficient charge transfer even at limited driving force.[42]

A possible explanation is that the IQE previously reported by us[12] was measured in short circuit conditions, which is in the presence of an internal electric field in the order of V_{BI}/d that can be approximated as V_{OC}/d, where V_{BI} is the built-in

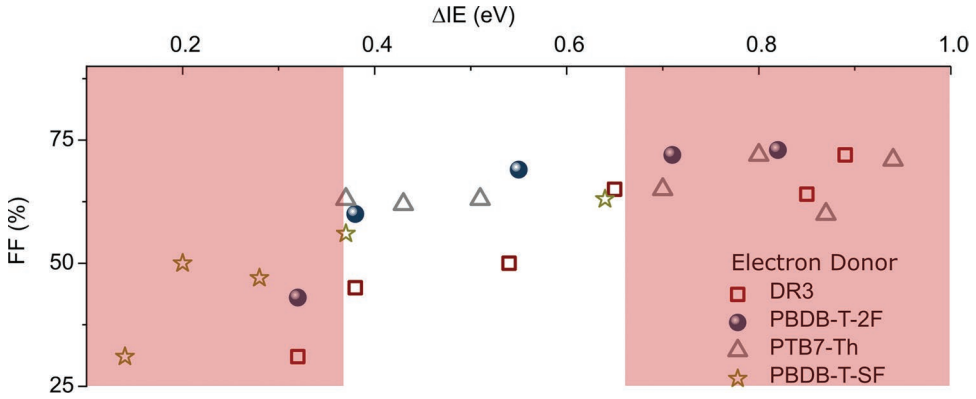

Figure 4. Fill factor of the donor–acceptor solar cells, the symbols represent the different donors, the detailed of the acceptors can be found in Figure S7, Supporting Information, the region of interest is in white background. Adapted from.[12] Copyright 2021, Springer.

potential of the solar cell and *d* its active layer thickness. This internal electric field could facilitate the hole transfer and/or stabilize (decrease) the CT state energy relative to the acceptor's exciton energy. If this was the case, one would expect the maximum photocurrent is reached only when the internal field is sufficiently strong, that is, at biases approaching short circuit conditions. This would result in poor fill factors (FF) in blends with ΔIE ≈ *0.4* eV, where the support of the internal electric field is required, and it would progressively increase toward ΔIE ≈ 0.6 eV, where the hole transfer would be energetically favorable even in the absence of any internal electric field.

The evolution of FF with ΔIE is depicted in **Figure 4**. Except for the DR3:acceptor systems, only a minimal increase of FF can be seen within that range, which practically rules out a field-assisted hole transfer process.

We note that the DR3:acceptor systems are different: a step-wise increase of the FF is visible in the device IQE (see Figure 2a). This was attributed to charge separation (distant to the interface CT state) being 100% efficient only at large enough offsets, in contrast to other D:acceptor systems, as indicated by the geminate recombination observed by transient absorption spectroscopy.[12] However, this requires further studies on a larger set of materials to reveal if this is a general feature of all-small molecules solar cells, which could explain the lower fill factor for a given ΔIE, or alternatively a larger ΔIE required, resulting in larger energy losses for example in evaporated solar cells.[43–46]

2.4. Discussion and Generalization

Excluding the impact of the solar cells' internal electric field, the question remains as to why, if the difference between E_{CT} and E_g^A is ≈0.45–0.6 eV (see Figure 3), an IE offset of ≈ 0.45–0.5 eV is sufficient to maximize the hole transfer efficiency, that is, the acceptor exciton to CT state transition.[12] A possible explanation is that the acceptor excitons' delocalization enables them to gradually hybridize with a CT state component already when the excitons approach the interface, thus allowing for a part of ΔE_b to be ignored, while another part is possibly included in the interfacial bias potential B.[40]

To verify the generality of our findings, we extended the energy loss calculation to 24 ternary blends and 52 binary blends taken from[12,20,21,36,38,47,48] (the details of the systems can be found in Figure S5, Supporting Information). As can be seen in **Figure 5**, all the binary blends and most of the ternaries follow the same trend. Notably, in five cases, the electron donor has a larger optical bandgap than the acceptor, and thus the energy losses were calculated from the donor's optical bandgap E^D_g. Moreover, in such a case, we expect that excitons generated in the acceptor undergo energy transfer to the donor, and as a result, the charge transfer should be dominated by electron transfer, and hence controlled by the materials' electron affinities and offsets ΔEA. To find out, we plotted the energy losses for those systems versus ΔEA. In fact, the trend is reproduced for those systems. Here, the systems were: PBDB-T:EH-IDTBR,[38] PTB7-Th:EH-IDTBR,[21]

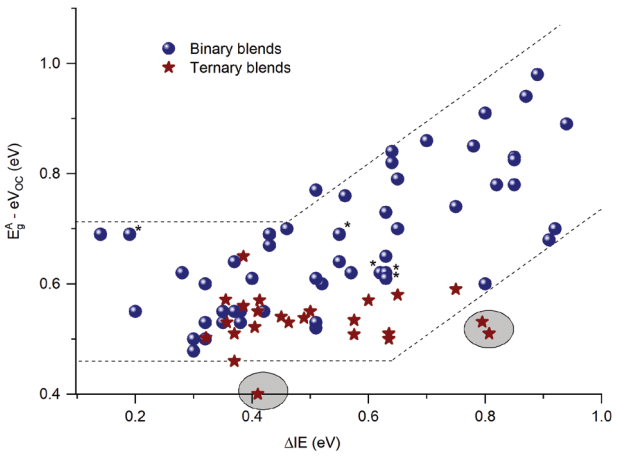

Figure 5. Energy losses between the lowest absorber optical bandgap and the solar cell open circuit voltage based on 26 ternary (one donor, two acceptors)[20] and 56 binary blends.[12,20,21,36,38,47,48] The details of the blends can be found in Figure S8, Supporting Information. For the five systems marked by an asterisk: PBDB-T:EH-IDTBR, PTB7-Th:EH-IDTBR, PTB7-Th:O-IDTBR, PffBT4T-2OD:FBR, and PffBT4T-2OD:IDFBR, the electron donor has a lower optical bandgap than the acceptor. For those cases, the energy loss was thus calculated from the donor bandgap, and plotted against the electron affinity offset. The shaded areas highlight the three outliers discussed further in the text.

PTB7-Th:EH-O-IDTBR,[12,36] PffBT4T-2OD:FBR,[21,38] and PffBT4T-2OD:IDFBR.[38] They are indicated by an asterisk (*) in Figure 5. Note that for the ternary blends, the energy offset was calculated as the difference between the ionization energy of the electron donor and the average of the acceptors ionization energies, weighted for their blending ratios, as reported earlier by us.[20]

Three outliers are highlighted in Figure 5: those three ternary blends are composed of a donor blended with an average band acceptor to which a small fraction of a lower bandgap acceptor (10% of the total acceptor weight) was added. The energy losses depicted in Figure 5 were calculated from this low bandgap acceptor and are thus lower than for the others that obey the trend. However, if calculated from the majority acceptor optical bandgap, the energy losses follow the trend. In other words, it appears that the ternary blending strategy enables to add a small fraction of a low bandgap absorber, without scarifying V_{OC}. Thus, this is a very promising strategy for high-efficiency organic solar cells. However, the trend is not observed in all ternary systems. Here, the three notable exceptions are: PBDB-T-2F:ICC6:IEICO, PBDB-T-2F: IEICO:COi8DFIC, and PBDB-T-2F:IT-4F:COi8DFIC with blending ratios of 1:0.9:0.1, but the same effect is not observed in PBDB-T-2F:IT-4F:IEICO when using the same blending ratio.

Finally, we would like to stress that for a given ΔIE (resp. ΔEA), the energy losses still vary by about 250 meV. These losses have previously been ascribed to radiative and non-radiative recombination losses[28] and are currently the subject of intensive investigations by the global OPV community. Among several explanations, the energy gap law implies that non-radiative losses increase as the bandgap of the state from which recombination occurs decreases,[49] and as we have discussed, this state could be the interface CT state, or the exciton of the blend's lowest bandgap component. In this context, the raise of the interface (CT) state energy levels due to the interfacial energy level bending[12,14] should limit the energy losses even more. Furthermore, it has also been shown that the hybridization of the interface (CT) state with the acceptor's excited (singlet) state contributes to reducing non-geminate recombination energy losses.[30] However, it has also been shown that this is compensated by a raise of the energy losses due to radiative recombination, resulting in an only marginal overall diminution of the total energy losses.[50] Last, it has also been demonstrated that more ordered[17,32] and more mixed[51] phases allow for lower energy losses.

3. Conclusion

To conclude, we have demonstrated that in donor–acceptor-based organic solar cells the difference between the ionization energy of the donor and that of the acceptor can be raised beyond the limit required for optimum internal quantum efficiency, without adding further energy losses. This gives rise to an optimum (sweet) range for ΔIE extending at most from 0.4 to 0.65 eV where the cells' quantum efficiency is maximized, while the energy losses remain minimal, or equivalently the short circuit current is maximized without decreasing V_{OC}, leading to a larger PCE.

We demonstrate that minimal energy losses for ΔIE below 0.6 eV are due to the fact that there is no energy loss from the photon absorption to the transition to the interface (CT) state, as $E_{CT} \geq E_g^A$. The reason why hole transfer can be unity in systems with ΔIE ranging from 0.45 to 0.6 eV in spite of $E_{CT} \geq E_g^A$ is yet to be understood. By closely examining the evolution of the device fill factor, we ruled out that the internal electric field assists charge generation increasing the short circuit current. Instead, we propose that hybridization between the CT state and the acceptor's exciton could play an important role. A notable exception was found in DR3:NFA systems, where the FF increases with ΔIE, which appears to be related to the incomplete charge separation, as previously reported in open circuit condition for ΔIE ≈0.4 eV. However, the question remains whether this is a general feature of all-small molecules D:A blends specific to the system studied here.

Finally, we extended the energy loss analysis to a total of 76 OPV systems, including ternary blends and several binary blends, for which the acceptor's bandgap is larger than that of the donor. We found that all those systems obey the same trend, provided that: i) the losses are calculated from the donor optical bandgap and plotted against ΔEA for the low E_g^d systems. ii) the ΔIE is calculated by using the average of both acceptor's IEs weighted for their blending ratios in ternary blends. A few notable exceptions however: in 3 of the ternaries studied here, where the lowest bandgap acceptor was a minority component (10%) of the blend, the energy losses correlated with the trend when considering the majority component instead of the lowest bandgap material. This indicates it is possible to obtain 10% from the absorption of a low-bandgap material, while maintaining the V_{OC} as high as if there was only a high-bandgap absorption, a very promising approach for future development.

4. Experimental Section

Most of the data presented here is gathered from previous publications:[12,20] for the original 23 systems,[21] for some of the energy levels, and[20,36,38] for the generalization. Only a few systems missing in the previous publications were added, or in cases of electroluminescence measurements, were re-measured (details in the support information) to obtain a better spectral sensitivity correction. For those system, the sample preparation, solar cells characterization, and electroluminescence spectroscopy methods are presented below. In addition, due to how critical those measurements are, we present again below how the ionization energy, electron affinity and optical bandgap were determined in.[12,20,21,36,38] Finally, the details of the fitting used to determine E_{CT} were presented in *section 2.2.* of this manuscript.

Sample Preparations: Most of the data was taken from existing publication. The few additional devices were prepared in an inverted device structure: ITO/ZnO/Active Layer/MoOx/Ag, for both the blends and pristine material cells. Zinc oxide (ZnO) was spin-coated over cleaned glass–ITO substrates for 30 s at 4000 rpm, providing a thickness of roughly 30 nm, after that, the as-cast films were thermally annealed at 150 °C for 10 min. Inside the glovebox, active layers material solutions were made by dissolving donor and acceptor in organic solvents (chloroform or chlorobenzene). Before being cast on the substrates, the prepared solutions were stirred over night at 40—60 °C. Using a controlled spin-coater from Specialty Coating Systems, the active layers were spin-cast from the solutions at 50 °C for 60 s. Then the active layers were annealed at 100—110 °C for 10 min. The samples were then loaded in a thermal evaporator to evaporate a 7 nm

molybdenum (VI) oxide MoO3 and a 100 nm Ag layer. The materials used were commercial materials with the exception of IDTTBM[52] and O-IDTBR[53] synthesized in KAUST. See suppliers details in Table S1, Supporting Information.

Solar Cells Characterization: *J–V* characteristics of solar cells were measured in a nitrogen-filled glovebox. Solar cells were illuminated with light from an Oriel Sol3A Class AAA solar simulator calibrated to 1 sun, AM1.5G, with a KG-5 silicon reference cell certified by Newport. A Keithley 2400 source meter was used to measure the *J–V* curves in the reverse direction, that is, from positive to negative bias with a dwell time of 10 ms.

Electroluminescence Spectroscopy: For the new EL measurements, the devices (active area of 0.1 cm^2) biased with d.c. voltages (Keithley 2420) similar to or lower than V_{OC} at 1 sun illumination or with a d.c. current similar or lower J_{SC} at 1 sun illumination. The emission was collected by a collimator inside a nitrogen-filled glovebox and guided to a spectrograph (Princeton Instruments SP2300) by an optical fiber. The spectrometer was equipped with a cooled Si CCD (Princeton Instruments PIX100BRX) and cooled InGaAs (Princeton Instruments PYR1024) camera. The system was wavelength calibrated with a Ne/Ar calibration light source (Princeton Instruments IntelliCal). The system's relative sensitivity was determined for the same central wavelength used in the measurement by measuring an ocean optics broad continuous spectrum light source (Ocean Optics HL-3P-CAL Calibrated Vis-NIR light source, 350 – 2400 nm).

Optical Bandgap Determination: The used optical bandgaps are taken from[12,21,38] where they were determined in neat material films as the intersection of the normalized photoluminescence and absorbance spectra, which corresponded to the 0-0 vibrational level of the electronic transition between the ground state and the excited state of the films.

Another useful estimate of the bandgap, in blends, was the inflexion point of the raise of the EQE spectra, as this bandgap definition was used to estimate the ideal cell V_{OC} under Shockley–Queisser theory.[54] This optical bandgap was calculated for the systems presented in[12] (EQE data available in[27]) and are presented in Table S2, Supporting Information, for comparison. The values were very close to those obtained in pristine material from the intersection of the normalized PL and the absorbance spectra, being typically just a bit lower by 0 to 90 meV (usually less than 50).

Ionization Energy and Electron Affinity: The used IE and EA are taken from[12,20,21,36] where they were determined by Ultraviolet Photoelectron Spectroscopy and Low Energy Photoelectron Spectroscopy. The full setup description can be found in.[12] As explained there:

"the low kinetic energy secondary electron cut-off was used to determine the sample work function WF. A linear extrapolation to the baseline allows approximate determination using the following equation:

$$KEe = h\nu - \phi - EB = 0 \quad (2)$$

where *KEe* is the photoelectron kinetic energy (equal to 0 at secondary electron cut-off), $h\nu$ is the excitation energy He(1) 21.22 eV, *EB* is the binding energy relative to the Fermi energy of a sputter-cleaned Ag foil, determined in a separate measurement and ϕ the work function to the local vacuum level. The estimated precision and spectra reproducibility is ±0.05 eV."

The method was further improved in,[21] as the linear extrapolation for the onset of the signal was replaced by a Gaussian fit of the signal, which offers a determination of the onset position less influenced by the noise and thus more reproducible (especially critical for the LE-IPES data where the signal to noise ratio is often an issue).

Internal Quantum Efficiency: The used IQE are taken from[12] where they were obtained as the spectral average of the IQE spectra, averaged over a range where the absorption is high enough to minimize the calculation errors (often 400–800 nm, the low energy boundary depending of the bandgap of the acceptor used). The IQE spectra was obtained from the EQE spectra as:

$$\mathrm{IQE}(\lambda) = \frac{\mathrm{EQE}(\lambda)}{1 - \mathrm{R\%} - \text{parasitic absorption}} \quad (3)$$

Where R% is the reflectance measured on a stack similar to the solar cell device (but deposited on an unpatterned Glass/ITO substrate) and the parasitic absorption is simulated using a transfer matrix matlab script freely available at https://web.stanford.edu/group/mcgehee/transfermatrix/ and developed by Burkhard et al.[55] Reference refractive indexes were used for the electrodes and transport layers, while the active layers were determined locally by ellipsometry.

This method had limitations: The EQE and R% spectra were obtained from different devices, while the parasitic absorption came from simulation, using reference refractive indexes for some layers, which might differ slightly from those used on the devices. As a result the estimated IQE spectra contained an optical correction error spectrum – more or less an interference pattern – superposed to the actual IQE, which was responsible for the unexpected waviness of the obtained spectra. However, this error contained positive and negative regions that largely cancel out upon spectral averaging, making the spectrally averaged IQE reliable values.

Supporting Information

Supporting Information is available from the Wiley Online Library or from the author.

Acknowledgements

The authors acknowledge the support of the King Abdullah University of Science and Technology (KAUST) Office of Sponsored Research (OSR) under Award No. CCF-3079.

Conflict of Interest

The authors declare no conflict of interest.

Data Availability Statement

The data that support the findings of this study are available in the Supporting Information of this article.

Keywords

design rules, energy losses, molecule performances predictability, organic photovoltaics, quantum efficiency

Received: December 25, 2022
Revised: February 14, 2023
Published online: March 29, 2023

[1] A. Armin, W. Li, O. J. Sandberg, Z. Xiao, L. Ding, J. Nelson, D. Neher, K. Vandewal, S. Shoaee, T. Wang, H. Ade, T. Heumüller, C. Brabec, P. Meredith, *Adv. Energy Mater.* **2021**, *11*, 2003570.
[2] NREL, Interactive Best Research-Cell Efficiency Chart https://www.nrel.gov/pv/interactive-cell-efficiency.html (accessed: March 2023).
[3] C. W. Tang, *Appl. Phys. Lett.* **1986**, *48*, 183.
[4] J. Yuan, Y. Zhang, L. Zhou, G. Zhang, H.-L. Yip, T.-K. Lau, X. Lu, C. Zhu, H. Peng, P. A. Johnson, M. Leclerc, Y. Cao, J. Ulanski, Y. Li, Y. Zou, *Joule* **2019**, *3*, 1140.
[5] B. Lu, J. Wang, Z. Zhang, J. Wang, X. Yuan, Y. Ding, Y. Wang, Y. Yao, *Nano Select* **2021**, *2*, 2029.

[6] Y. Firdaus, V. M. Le Corre, J. I. Khan, Z. Kan, F. Laquai, P. M. Beaujuge, T. D. Anthopoulos, *Adv. Sci.* **2019**, *6*, 1802028.
[7] Y. Lin, M. I. Nugraha, Y. Firdaus, A. D. Scaccabarozzi, F. Aniés, A.-H. Emwas, E. Yengel, X. Zheng, J. Liu, W. Wahyudi, E. Yarali, H. Faber, O. M. Bakr, L. Tsetseris, M. Heeney, T. D. Anthopoulos, *ACS Energy Lett.* **2020**, *5*, 3663.
[8] O. J. Sandberg, A. Armin, *J. Phys. Chem. C* **2021**, *125*, 15590.
[9] Z. Zheng, J. Wang, P. Bi, J. Ren, Y. Wang, Y. Yang, X. Liu, S. Zhang, J. Hou, *Joule* **2022**, *6*, 171.
[10] Y. Cui, Y. Xu, H. Yao, P. Bi, L. Hong, J. Zhang, Y. Zu, T. Zhang, J. Qin, J. Ren, Z. Chen, C. He, X. Hao, Z. Wei, J. Hou, *Adv. Mater.* **2021**, *33*, 2102420.
[11] Y. Lin, Y. Firdaus, F. H. Isikgor, M. I. Nugraha, E. Yengel, G. T. Harrison, R. Hallani, A. El-Labban, H. Faber, C. Ma, X. Zheng, A. Subbiah, C. T. Howells, O. M. Bakr, I. McCulloch, S. de Wolf, L. Tsetseris, T. D. Anthopoulos, *ACS Energy Lett.* **2020**, *5*, 2935.
[12] S. Karuthedath, J. Gorenflot, Y. Firdaus, N. Chaturvedi, C. S. P. de Castro, G. T. Harrison, J. I. Khan, A. Markina, A. H. Balawi, T. A. D. Peña, W. Liu, R.-Z. Liang, A. Sharma, S. H. K. Paleti, W. Zhang, Y. Lin, E. Alarousu, S. Lopatin, D. H. Anjum, P. M. Beaujuge, S. de Wolf, I. McCulloch, T. D. Anthopoulos, D. Baran, D. Andrienko, F. Laquai, *Nat. Mater.* **2021**, *20*, 378.
[13] N. B. Kotadiya, A. Mondal, P. W. M. Blom, D. Andrienko, G.-J. A. H. Wetzelaer, *Nat. Mater.* **2019**, *18*, 1182.
[14] A. Markina, K.-H. Lin, W. Liu, C. Poelking, Y. Firdaus, D. R. Villalva, J. I. Khan, S. H. K. Paleti, G. T. Harrison, J. Gorenflot, W. Zhang, S. de Wolf, I. McCulloch, T. D. Anthopoulos, D. Baran, F. Laquai, D. Andrienko, *Adv. Energy Mater.* **2021**, *11*, 2102363.
[15] C. Poelking, D. Andrienko, *J. Am. Chem. Soc.* **2015**, *137*, 6320.
[16] L. E. Sousa, V. Coropceanu, D. A. da Silva Filho, G. Sini, *Adv. Theory Simul.* **2020**, *3*, 2070008.
[17] C. Poelking, M. Tietze, C. Elschner, S. Olthof, D. Hertel, B. Baumeier, F. Würthner, K. Meerholz, K. Leo, D. Andrienko, *Nat. Mater.* **2015**, *14*, 434.
[18] C. Poelking, D. Andrienko, *J. Chem. Theory Comput.* **2016**, *12*, 4516.
[19] L. Perdigón-Toro, H. Zhang, A. Markina, J. Yuan, S. M. Hosseini, C. M. Wolff, G. Zuo, M. Stolterfoht, Y. Zou, F. Gao, D. Andrienko, S. Shoaee, D. Neher, *Adv. Mater.* **2020**, *32*, 1906763.
[20] S. Karuthedath, S. H. K. Paleti, A. Sharma, H. Yin, C. S. P. de Castro, S. Chen, H. Xu, N. Alshehri, N. Ramos, J. I. Khan, J. Martin, G. Li, F. Laquai, D. Baran, J. Gorenflot, *Adv. Energy Mater.* **2023**, https://doi.org/10.1002/aenm.202203464.
[21] J. Bertrandie, J. Han, C. S. P. de Castro, E. Yengel, J. Gorenflot, T. Anthopoulos, F. Laquai, A. Sharma, D. Baran, *Adv. Mater.* **2022**, *34*, 2202575.
[22] J. Zhang, W. Liu, G. Zhou, Y. Yi, S. Xu, F. Liu, H. Zhu, X. Zhu, *Adv. Energy Mater.* **2020**, *10*, 1903298.
[23] C. He, Y. Pan, Y. Ouyang, Q. Shen, Y. Gao, K. Yan, J. Fang, Y. Chen, C.-Q. Ma, J. Min, C. Zhang, L. Zuo, H. Chen, *Energy Environ. Sci.* **2022**, *15*, 2537.
[24] X. Li, Q. Zhang, J. Yu, Y. Xu, R. Zhang, C. Wang, H. Zhang, S. Fabiano, X. Liu, J. Hou, F. Gao, M. Fahlman, *Nat. Commun.* **2022**, *13*, 2046.
[25] C. Deibel, D. Mack, J. Gorenflot, A. Schöll, S. Krause, F. Reinert, D. Rauh, V. Dyakonov, *Phys. Rev. B* **2010**, *81*, 85202.
[26] J. Kern, S. Schwab, C. Deibel, V. Dyakonov, *Phys. Status Solidi RRL* **2011**, *5*, 364.
[27] J. Gorenflot, S. Karuthedath, Y. Firdaus, N. Chaturvedi, C. S. P. de Castro, G. T. Harrison, J. I. Khan, A. Markina, A. H. Balawi, T. A. Dela Peña, W. Liu, R.-Z. Liang, A. Sharma, S. H. K. Paleti, W. Zhang, Y. Lin, E. Alarousu, D. H. Anjum, P. M. Beaujuge, S. de Wolf, I. McCulloch, T. D. Anthopoulos, D. Baran, D. Andrienko, F. Laquai, *Nature Materials – NM19093092C – shared data*, https://figshare.com/collections/Nature_Materials_-_NM19093092C_-_shared_data/5110076/1 (accessed: March 2023).
[28] K. Vandewal, K. Tvingstedt, A. Gadisa, O. Inganäs, J. V. Manca, *Phys. Rev. B* **2010**, *81*, 125204.
[29] L. Perdigón-Toro, Q. L. Phuong, S. Zeiske, K. Vandewal, A. Armin, S. Shoaee, D. Neher, *ACS Energy Lett.* **2021**, *6*, 557.
[30] F. D. Eisner, M. Azzouzi, Z. Fei, X. Hou, T. D. Anthopoulos, T. J. S. Dennis, M. Heeney, J. Nelson, *J. Am. Chem. Soc.* **2019**, *141*, 6362.
[31] K. Nakano, Y. Chen, B. Xiao, W. Han, J. Huang, H. Yoshida, E. Zhou, K. Tajima, *Nat. Commun.* **2019**, *10*, 2520.
[32] S.-U.-Z. Khan, J. Bertrandie, M. Gui, A. Sharma, W. Alsufyani, J. F. Gorenflot, F. Laquai, D. Baran, B. P. Rand, *Joule* **2022**, *6*, 2821.
[33] S.-U.-Z. Khan, B. P. Rand, *Phys. Rev. Appl.* **2021**, *16*, 44026.
[34] C. Göhler, C. Deibel, *ACS Energy Lett.* **2022**, *7*, 2156.
[35] J. Yan, E. Rezasoltani, M. Azzouzi, F. Eisner, J. Nelson, *Nat. Commun.* **2021**, *12*, 3642.
[36] J. I. Khan, M. A. Alamoudi, N. Chaturvedi, R. S. Ashraf, M. N. Nabi, A. Markina, W. Liu, T. A. Dela Peña, W. Zhang, O. Alévêque, G. T. Harrison, W. Alsufyani, E. Levillain, S. de Wolf, D. Andrienko, I. McCulloch, F. Laquai, *Adv. Energy Mater.* **2021**, *11*, 2100839.
[37] A. Classen, C. L. Chochos, L. Lüer, V. G. Gregoriou, J. Wortmann, A. Osvet, K. Forberich, I. McCulloch, T. Heumüller, C. J. Brabec, *Nat. Energy* **2020**, *5*, 711.
[38] Y. Dong, H. Cha, H. L. Bristow, J. Lee, A. Kumar, P. S. Tuladhar, I. McCulloch, A. A. Bakulin, J. R. Durrant, *J. Am. Chem. Soc.* **2021**, *143*, 7599.
[39] Y. Liu, Z. Zheng, V. Coropceanu, J.-L. Brédas, D. S. Ginger, *Mater. Horiz.* **2022**, *9*, 325.
[40] X.-K. Chen, V. Coropceanu, J.-L. Brédas, *Nat. Commun.* **2018**, *9*, 5295.
[41] M. List, T. Sarkar, P. Perkhun, J. Ackermann, C. Luo, U. Würfel, *Nat. Commun.* **2018**, *9*, 3631.
[42] Y. Zhong, M. Causa', G. J. Moore, P. Krauspe, B. Xiao, F. Günther, J. Kublitski, R. Shivhare, J. Benduhn, E. BarOr, S. Mukherjee, K. M. Yallum, J. Réhault, S. C. B. Mannsfeld, D. Neher, L. J. Richter, D. M. DeLongchamp, F. Ortmann, K. Vandewal, E. Zhou, N. Banerji, *Nat. Commun.* **2020**, *11*, 833.
[43] P. Kaienburg, A. Jungbluth, I. Habib, S. V. Kesava, M. Nyman, M. K. Riede, *Adv. Mater.* **2022**, *34*, 2107584.
[44] I. Ramirez, M. Causa', Y. Zhong, N. Banerji, M. Riede, *Adv. Energy Mater.* **2018**, *8*, 1703551.
[45] M. Riede, D. Spoltore, K. Leo, *Adv. Energy Mater.* **2021**, *11*, 2002653.
[46] A. Venkateswararao, K.-T. Wong, *Bull. Chem. Soc. Jpn.* **2021**, *94*, 812.
[47] S. Li, L. Ye, W. Zhao, S. Zhang, S. Mukherjee, H. Ade, J. Hou, *Adv. Mater.* **2016**, *28*, 9423.
[48] H. Yao, L. Ye, J. Hou, B. Jang, G. Han, Y. Cui, G. M. Su, C. Wang, B. Gao, R. Yu, H. Zhang, Y. Yi, H. Y. Woo, H. Ade, J. Hou, *Adv. Mater.* **2017**, *29*, 1700254.
[49] J. Benduhn, K. Tvingstedt, F. Piersimoni, S. Ullbrich, Y. Fan, M. Tropiano, K. A. McGarry, O. Zeika, M. K. Riede, C. J. Douglas, S. Barlow, S. R. Marder, D. Neher, D. Spoltore, K. Vandewal, *Nat. Energy* **2017**, *2*, 17053.
[50] T. A. Dela Peña, J. I. Khan, N. Chaturvedi, R. Ma, Z. Xing, J. Gorenflot, A. Sharma, F. L. Ng, D. Baran, H. Yan, F. Laquai, K. S. Wong, *ACS Energy Lett.* **2021**, *6*, 3408.

[51] K. D. Rosenthal, M. P. Hughes, B. R. Luginbuhl, N. A. Ran, A. Karki, S.-J. Ko, H. Hu, M. Wang, H. Ade, T.-Q. Nguyen, *Adv. Energy Mater.* **2019**, *9*, 1901077.
[52] R.-Z. Liang, M. Babics, A. Seitkhan, K. Wang, P. B. Geraghty, S. Lopatin, F. Cruciani, Y. Firdaus, M. Caporuscio, D. J. Jones, P. M. Beaujuge, *Adv. Funct. Mater.* **2018**, *28*, 1705464.
[53] S. Holliday, R. S. Ashraf, A. Wadsworth, D. Baran, S. A. Yousaf, C. B. Nielsen, C.-H. Tan, S. D. Dimitrov, Z. Shang, N. Gasparini, M. Alamoudi, F. Laquai, C. J. Brabec, A. Salleo, J. R. Durrant, I. McCulloch, *Nat. Commun.* **2016**, *7*, 11585.
[54] U. Rau, B. Blank, T. C. M. Müller, T. Kirchartz, *Phys. Rev. Appl.* **2017**, *7*, 044016.
[55] G. F. Burkhard, E. T. Hoke, M. D. McGehee, *Adv. Mater.* **2010**, *22*, 3293.